Delft University of Technology

Thermal imaging analysis of ballast fouling
Investigating the effects of parent rock and fouling materials through IRT passive camera

Koohmishi, Mehdi; Kaewunruen, Sakdirat; Jing, Guoqing; Guo, Yunlong

Important note
To cite this publication, please use the final published version (if applicable).
Please check the document version above.

Original Article

Thermal imaging analysis of ballast fouling: Investigating the effects of parent rock and fouling materials through IRT passive camera

Mehdi Koohmishi [a], Sakdirat Kaewunruen [b], Guoqing Jing [c], Yunlong Guo [d,e,*]

[a] *Department of Civil Engineering, Faculty of Engineering, University of Bojnord, Bojnord, Iran*
[b] *Department of Civil Engineering, School of Engineering, University of Birmingham, Birmingham B152TT, United Kingdom*
[c] *School of Civil Engineering, Beijing Jiaotong University, Beijing 100044, China*
[d] *Faculty of Civil Engineering and Geosciences, Delft University of Technology, Delft 2628CN, Netherlands*
[e] *Department of Civil Engineering, School of Engineering, University of Birmingham, Birmingham B152TT, United Kingdom*

ABSTRACT

This study explores the use of infrared thermography (IRT) technology for the non-destructive evaluation of ballast fouling in railway tracks, focusing on the influence of parent rock types and fouling materials. Utilizing thermal imaging, the research investigates how variations in ballast conditions affect surface temperature, which serves as an indicator of structural integrity and health. The experimental setup involved ballast samples derived from three different rock types—basalt, limestone, and andesite—fouled with commonly encountered materials like sand and clay at varying percentages. Results demonstrate that fouling level and type significantly influence the thermal signatures captured by IRT passive camera. Notably, ballast derived from darker rocks exhibited higher temperatures, indicating greater emissivity, while fouled ballast showed distinct temperature patterns compared to clean samples, emphasizing the potential of thermal imaging in detecting and quantifying fouling in ballast layers. This research underscores the viability of IRT passive camera in the routine maintenance and monitoring of railway infrastructure, providing a foundation for further development of integrated diagnostic tools for railway management systems.

Introduction

Railway ballasted tracks are globally recognized as the backbone for rail transportation infrastructure. The ballast layer, comprised of large-sized crushed rocks with angular and rough surfaces, plays multiple critical roles, including facilitating drainage throughout the structure and enabling adjustments to track geometry and stiffness throughout its lifespan [25,32]. Despite its benefits, the presence of fouling—arising from particle degradation or the incursion of external materials like subgrade soil, coal, and wind-blown sand—constitutes a pervasive defect, diminishing the ballast's functionality, notably its drainage capacity.

Railway track assessments, including the ballast layer, are in their nascent stages, focusing primarily on the diagnosis and prognosis of the superstructure and substructure conditions. Various non-destructive testing (NDT) methods have been employed to enhance the structural health monitoring of these tracks, including ground-penetrating radar, train-mounted sensors, and infrared thermography (IRT)

[9,56,37,12,18].

Infrared Thermography (IRT), also known as thermal imaging, is a standout among these techniques, providing a temperature-based analysis to support infrastructure health monitoring, particularly for railway tracks. This method involves detecting infrared energy emitted by objects, converting it to temperature, and visualizing it through color-coded images—cooler areas in blue and warmer areas in red [53]. The Forward-Looking Infrared Radiometer (FLIR) is a widely adopted tool for capturing these thermal images and identifying temperature differentials [21,10].

IRT has been validated as a highly effective technology for assessing the structural conditions of various civil engineering assets, as demonstrated through its diverse applications:

- Dhakal and Elseifi [16] effectively used IRT to detect segregation in asphalt overlays and the potential for reflective cracking, crucial for preventive maintenance planning. Pozzer et al.[54] utilized IRT-derived thermograms to calibrate a finite element model that
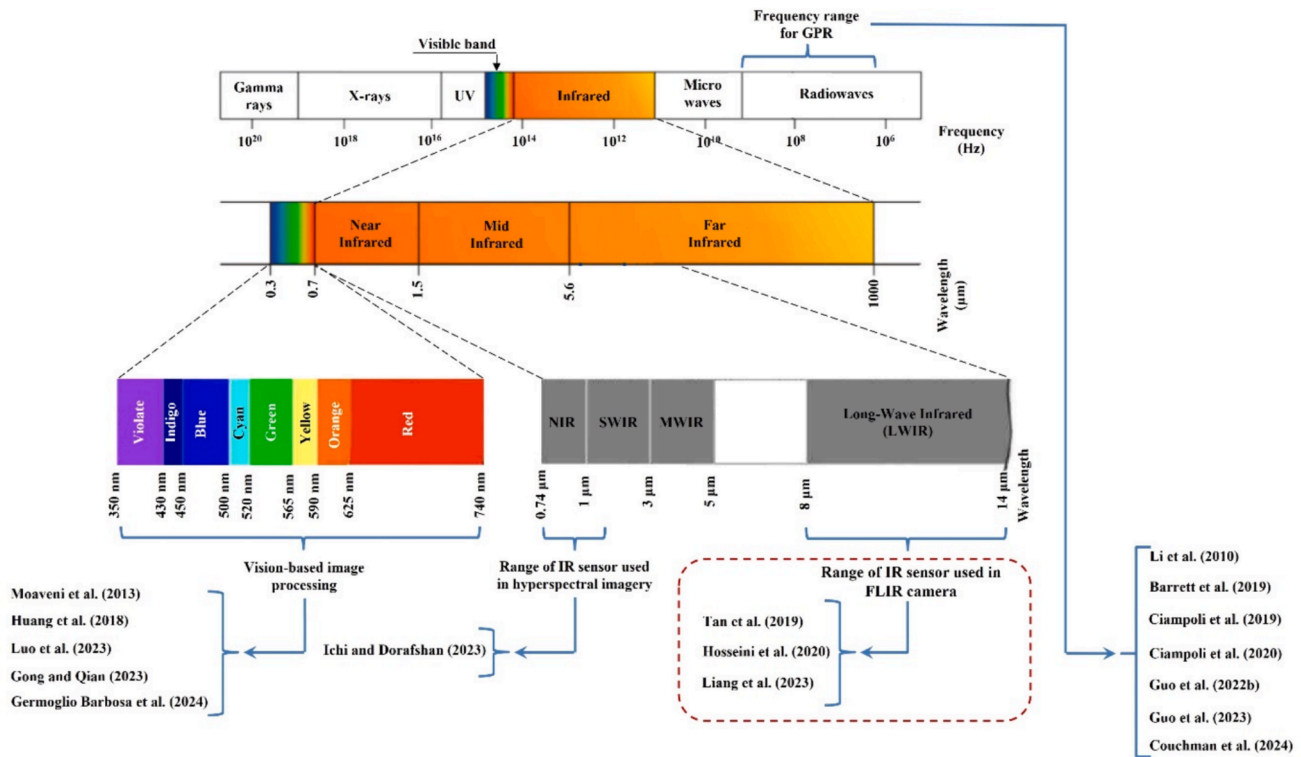
Fig. 1. Infrared wavelength intervals and characterized range for IRT: Classifying NDTs conducted on railway ballast based on electromagnetic spectrum [38,3,48,64,30,59,8,11,12,29,47,42,26,27,24,39,43,31,15,23].

Table 1
General properties of rock-type ballast derived from distinct queries.

Rock type	Color	Water absorption[1] (%)	LAAI[2] (%)
Limestone	Light grayish white	0.55	22.6
Basalt	Gray	0.56	18.5
Andesite	Dark purple	0.39	23.0

[1] Astm [7].
[2] Los Angeles abrasion index Astm [6].

detects subsurface delamination in concrete bridge decks. The analysis also optimized the timing for conducting thermographic inspections, enhancing maintenance accuracy and timing.

- Employing a combination of IRT and advanced image processing techniques, Kulkarni et al.[35] identified subsurface voids in roadways that were indicative of underlying culvert failures, thereby preventing potential road collapses. In a further study, Kulkarni et al. [36] implemented unmanned aerial vehicles (UAVs) to capture thermal images of pavement surfaces, significantly improving the efficiency and coverage of road health assessments.
- Almutawa and Eid [4] discovered an inverse relationship between soil moisture content and surface temperature using IRT. This finding indicates that an increase in moisture content, which raises the soil's specific heat capacity, results in a reduced temperature differential, thus providing critical insights into soil conditions [58].

IRT has demonstrated substantial success in the field of railway infrastructure as well. The utility of this technology extends across various types of railway tracks, evidencing its versatility and effectiveness.

- Slab tracks. Ye et al. [66] applied IRT along with an edge-detection algorithm to identify surface cracks on slab tracks. This method allowed for precise detection of flaws by analyzing the thermal

images of the slab surfaces, showcasing IRT's capability in pin-pointing structural vulnerabilities.
- Ballasted tracks. In a seminal study, Clark et al. [13] explored the use of IRT to monitor the condition of railway ballast, particularly to identify varying levels of fouling. This included the use of a FLIR camera equipped with an infrared detector which proved effective in discerning temperature variations associated with different fouling intensities. Subsequent studies, such as those by Tan et al. [59] and Hosseini et al. [29], expanded on this foundation with both laboratory and field tests under static and dynamic conditions.
- Comprehensive fouling detection: Liang et al.[39] further refined the application of IRT in detecting ballast fouling. Their work included detailed analysis of surface temperatures and involved mixing ballast with common fouling materials such as gravel and sand at fouling degrees of 0 %, 20 %, and 40 %, thereby enhancing the understanding of fouling impacts on thermal properties.

Additionally, the potential for integrating IRT with other NDT methods like ground penetrating radar and interferometric synthetic aperture radar has been recognized [17,34]. Such integrations promise to advance the comprehensiveness and accuracy of subsurface diagnostics, supporting a multi-scale, multi-physics approach to infrastructure analysis. In this regard, Fig. 1 categorizes the NDT methods used in railway ballast evaluation, including IRT, based on the electromagnetic spectrum. This classification helps in understanding the diverse approaches and their respective applications in maintaining and monitoring railway infrastructure integrity.

The comprehensive review on the potential applications of IRT for infrastructure inspection underscores the critical influencing factors that impact its accuracy and detectability. These factors are crucial for optimizing data acquisition processes, as detailed by Garrido et al. [22] and Tomita and Chew [61]. While ground penetrating radar has been established as a robust method for evaluating railway ballast cleanliness [40], IRT uniquely contributes by providing insights into the surface conditions of railway ballasted tracks.

a.1 Limestone　　　　　　**a.2** Basalt　　　　　　**a.3** Andesite

a Clean ballast particles

b.1 Sand　　　　　　　　　　　　**b.2** Clay

b Fouling materials

Fig. 2. Materials used in the present study.
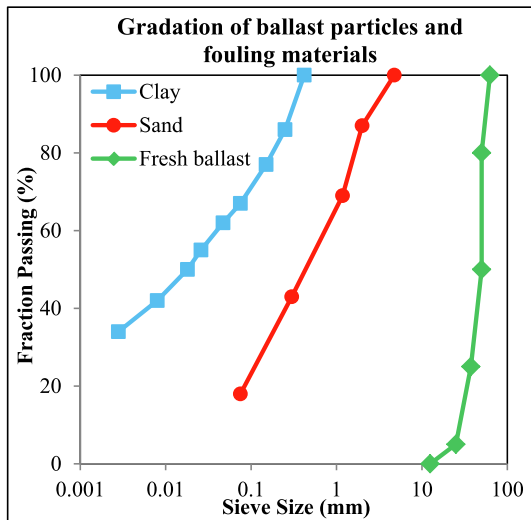
Fig. 3. Gradation curves of fresh crushed ballast particles and fouling materials.

Previous studies have leveraged thermal imaging to investigate ballast contamination effectively [59,29,39]. However, significant challenges remain in utilizing this technology for comprehensive ballast layer health monitoring. These challenges primarily arise from the varying effects of parent rock types and fouling materials on the thermal readings.

In response to these challenges, the primary objective of this study is to assess the capabilities of thermal imaging for the nondestructive evaluation of ballast fouling, with a particular focus on the impacts of parent rock types and fouling materials. To achieve this, a comprehensive set of experiments was conducted:

- The experiments were designed to measure thermal radiation from both clean and fouled ballast samples. These samples were systematically prepared with varying concentrations of common fouling materials such as clay and sand as well as providing both dry and wet conditions. Using a thermography camera, we recorded the surface temperatures of these samples to analyze the thermal effects of different fouling levels.
- Additionally, the study considered the influence of different parent rocks on thermal readings. Ballast particles from various rock sources were tested to identify any discrepancies in thermal behavior attributable to rock type. This aspect of the research helps in understanding how different geological backgrounds can affect the outcomes of thermal imaging.
- The methodology involved rigorous laboratory testing of the prepared ballast samples using IRT technology. This was done to simulate real-world conditions where different types of ballast and fouling materials are present, thereby enhancing the realism and applicability of the findings.
- The diverse conditions tested in these experiments reflect common scenarios encountered in railway asset management. This approach ensures that the IRT-based assessments developed here can be effectively translated into practical strategies for maintaining and monitoring railway infrastructures.
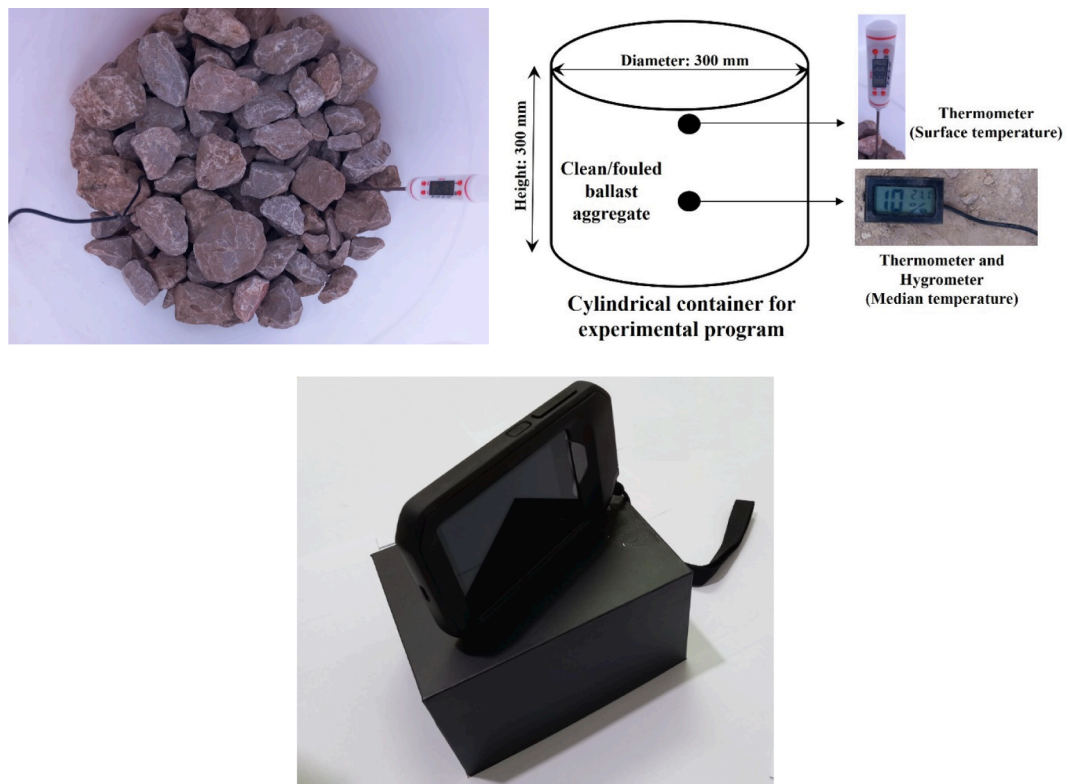
a Instruments used for conducting the experimental program

Fig. 4. FLIR camera used for capturing thermal images and prepared samples.
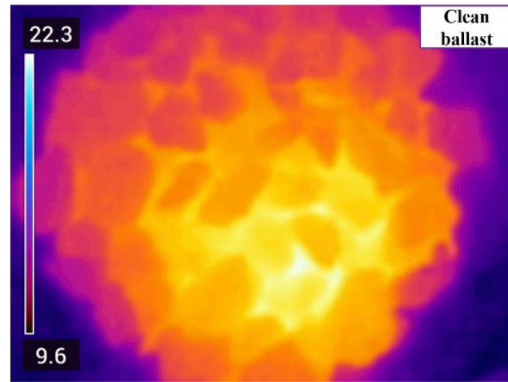
A visible light image   A thermal image

b.1 Rock type: Limestone
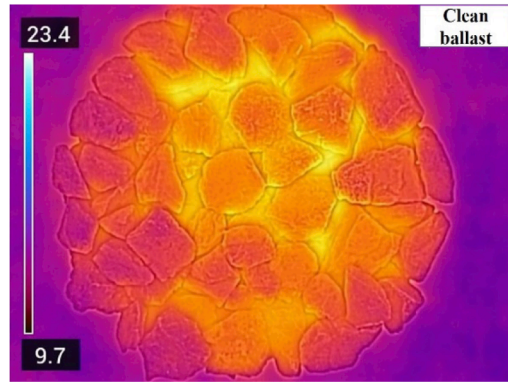
A visible light image   A thermal image

b.2 Rock type: Basalt
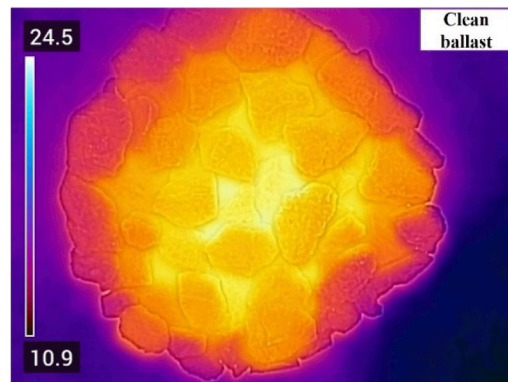
A visible light image   A thermal image

b.3 Rock type: Andesite

b Clean ballast samples: visible light and infrared thermal images

Fig. 4. (*continued*).

FR: 20%

FR: 20%
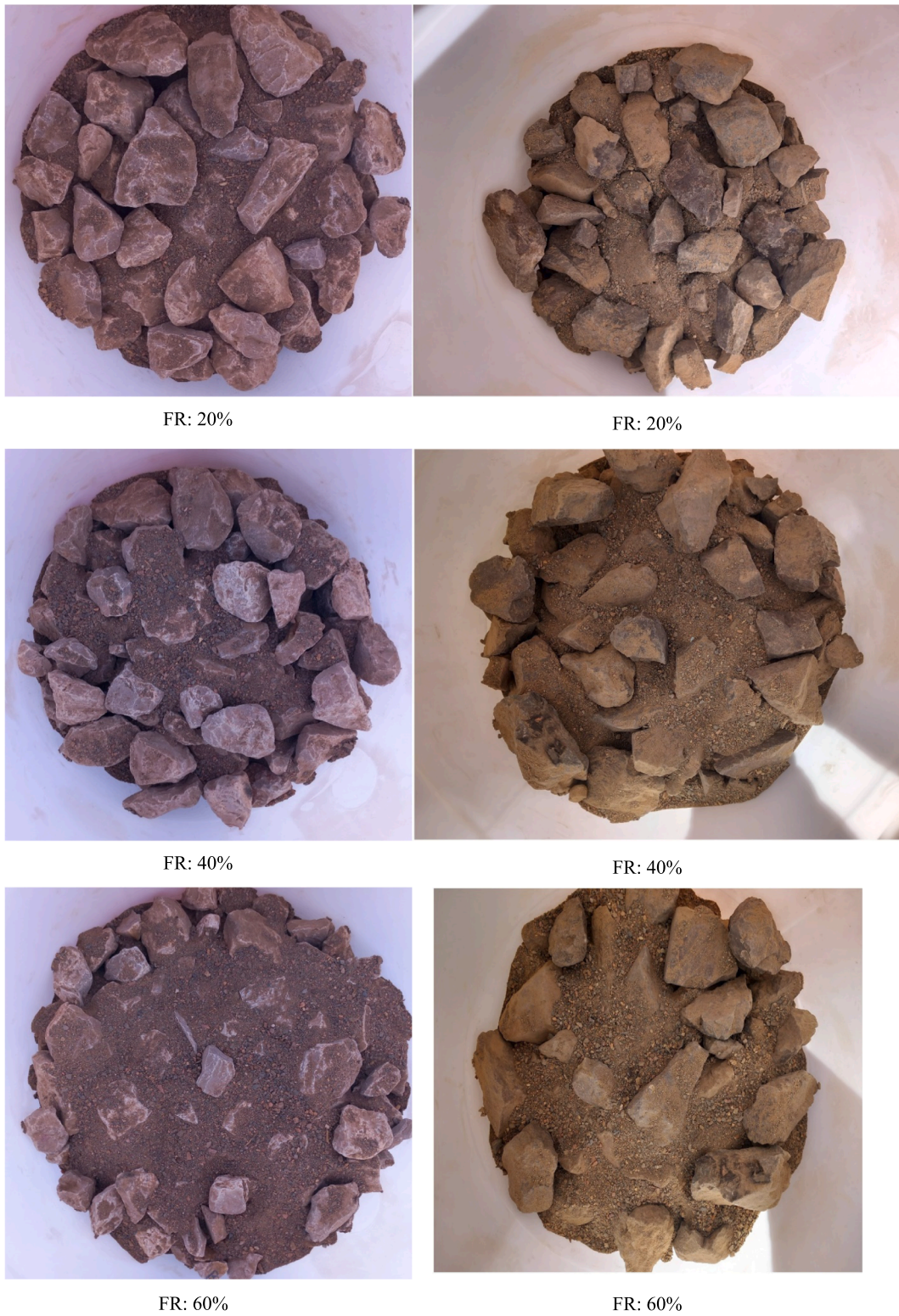
FR: 40%

FR: 40%

FR: 60%

FR: 60%

a.1 Rock type: Limestone

a.2 Rock type: Andesite

a Fouling material: Sand

Fig. 5. Ballast particles fouled with characterized fouling materials inside the cylindrical container.

FR: 20%

FR: 20%

FR: 40%
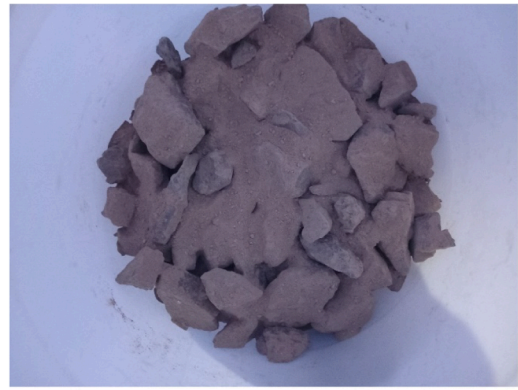
FR: 40%

FR: 60%

FR: 60%

b.1 Rock type: Limestone

b.2 Rock type: Andesite

b Fouling material: Clay

Fig. 5. (*continued*).

Materials and instruments

Railway ballast

Ballast particles obtained from three queries are used to consider the influence of parent rock. Table 1 presents the physical and mechanical properties of railway ballast particles derived from various parent rocks, namely limestone, basalt and andesite. Fig. 2.a shows the clean ballast samples derived from three distinct parent rock types. Furthermore,

Fig. 3 depicts the gradation curve established for fresh ballast particles.

Fouling materials

The present study considers sand and clay as fouling materials, as indicated by the gradation curve illustrated in Fig. 3. Moreover, Fig. 2.b illustrates the two types of fouling materials.
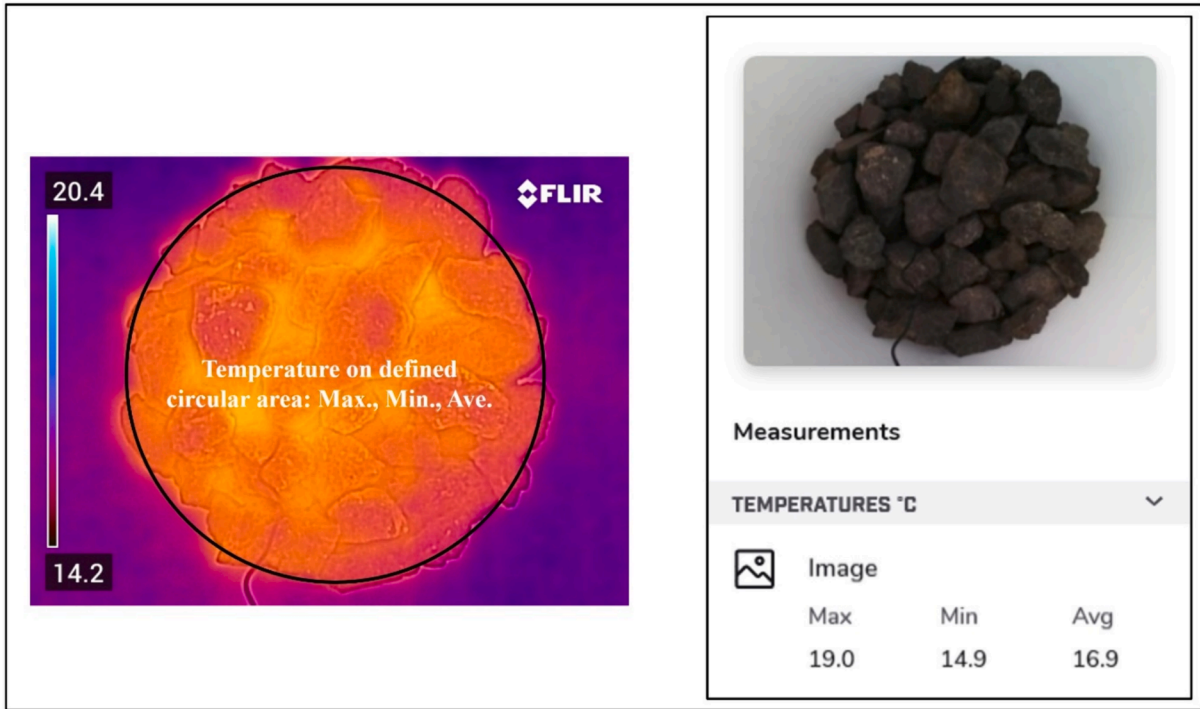
a Computation of average surface temperature: using FLIR thermal studio
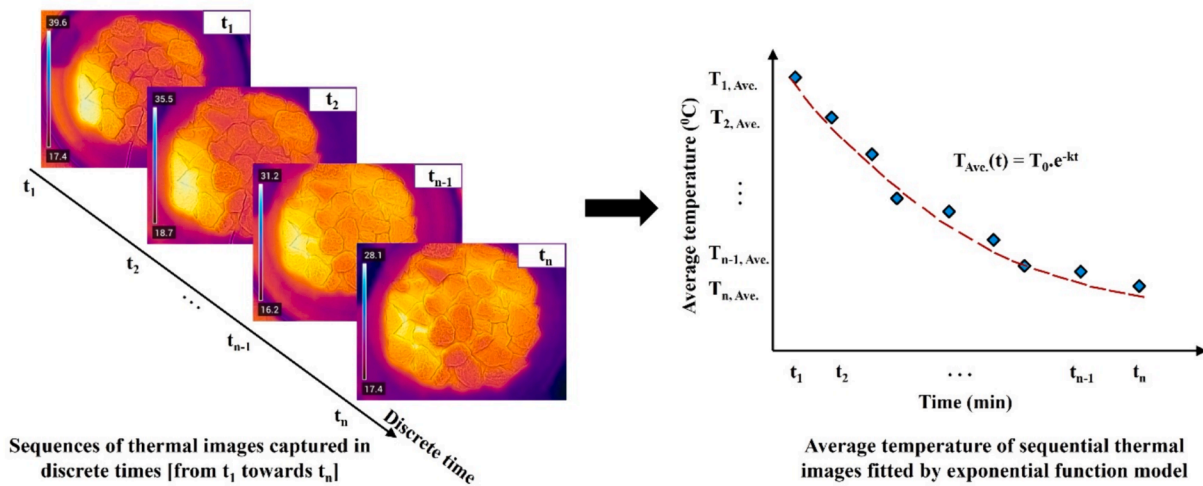
b Computation of temperature variation based on sequential images taken
from sample surface within a limited period

Fig. 6. Process of implementing analysis on surface temperature based on the IRT images.
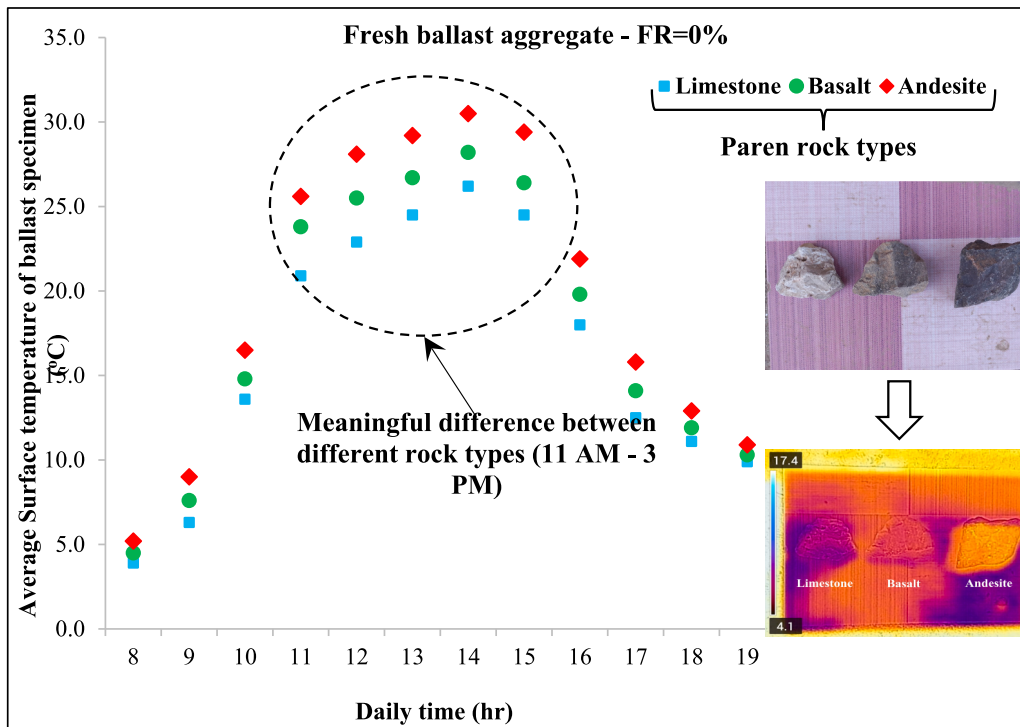
Fig. 7. Effect of parent rock on surface temperature of clean ballast particles.

Instruments and testing procedure

An infrared thermal imaging device, the FLIR C3-X, as illustrated in Fig. 4.a, operates within the 7.5–13 μm spectral range. This device is utilized to capture thermal images of ballast samples, both clean and fouled. The camera offers a resolution of 96 × 128 pixels and can measure temperatures ranging from −20 °C to 150 °C with an accuracy of ± 0.1 °C. The emissivity value recommended by FLIR [19] is adopted for accurate thermal readings. Additionally, to monitor environmental conditions during testing, both a thermometer and a hygrometer are utilized. These instruments measure the temperature and humidity levels at the center and on the surface of the ballast samples, providing essential data for accurate analysis.

IRT typically utilizes two distinct methodologies: active and passive thermography. The active method uses an artificial heat source, like a halogen lamp, to provide a controlled heating scenario. The other is passive thermography, which relies on natural sources of heat such as solar energy to excite the subjects of study, see ref. [45,62]. In this study, the passive method is employed. This setup ensures that both natural and enhanced environmental conditions are considered, providing a comprehensive analysis of the thermal properties of the ballast under varied circumstances.

To prepare the compacted samples of ballast particles in the laboratory-scale testing program, multiple large cylindrical containers with a diameter of 300 mm and a height of 300 mm are employed, as depicted in Fig. 4a. The weight of the fresh ballast particles used for each test ranges from 32 to 35 kg. Following the insights of Pappalardo and Mineo [51], using a cylindrical shape for the sample container is preferred over a prismatic shape due to its benefits in reducing boundary/edge effects. This geometric advantage is crucial as it minimizes distortions in the thermal imaging process.

The ballast particles placed inside the containers are exposed to direct sunlight to determine the thermal properties by employment of IRT technology. As illustrated in Fig. 4.b for three different rock types, the thermal images are reproduced using ironbow palette to represent a steady brightness and color gradient from higher temperature towards lower one. In this regard, brighter colors, like yellow, indicate warmer

temperatures, whilst the purple, dark blue and black represent cooler temperatures. Observations from the thermal images of these ballast samples indicate that cooling predominantly occurs at a faster rate at the sample's boundary compared to its core. This pattern aligns with findings from IRT studies on cylindrical soil samples [41], underscoring the consistency of thermal behaviors across different material types.

Quantification of ballast fouling due to intrusion of external materials

To quantify the level of intrusion of sand and clay, representing external fouling materials, among the ballast particles, the fouling ratio is computed as follows:

$$FR = \frac{M_F}{M_B} \times 100 \tag{1}$$

FR = Fouling ratio (%)
    M_F = Dry mass of the fouling material (kg).
    M_B = Dry mass of the clean ballast sample (kg).
    In this paper, FR values of 20 %, 40 %, and 60 % along with the clean ballast samples (0 % FR) were prepared, as illustrated in Fig. 5.

Surface temperature analysis of ballast

Post-processing techniques are applied to raw infrared images to extract statistical data for the quantification of surface temperatures. Fig. 6 illustrates the two principal methods used for this purpose:

1 Average surface temperature: The software in [20] is employed to calculate the average surface temperature across the entire sample area (see Fig. 6.a). This tool provides a straightforward and reliable means to gauge the general thermal state of the sample.

2 Regression analysis on thermographic sequences: For a more detailed temporal analysis, the average temperature is computed for various sequences of thermal images captured at discrete times. These data are then analyzed to determine how the temperature varies over time, using an exponential trendline to model these changes [65,55] (see Fig. 6.b). This method allows for an in-depth understanding of the
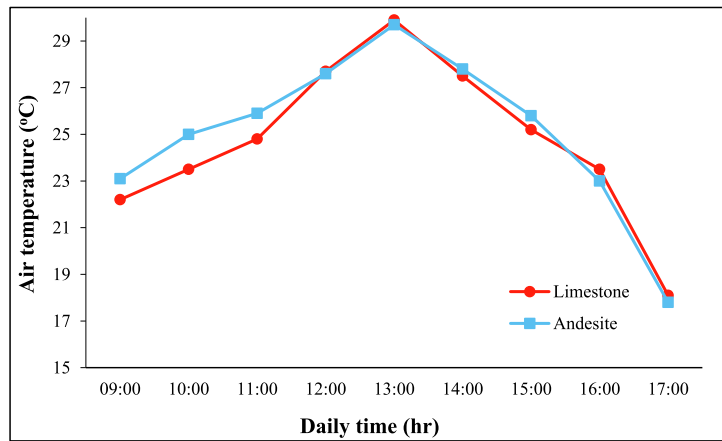
a Air temperature
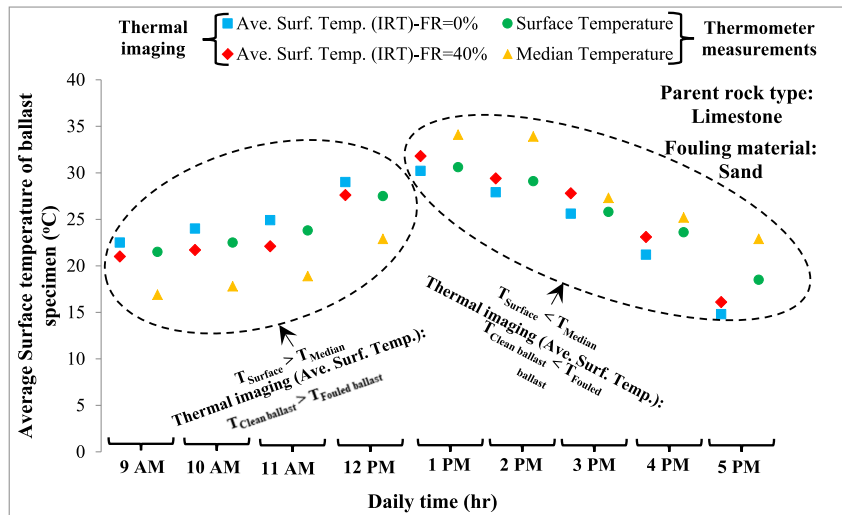
b Rock type: Limestone
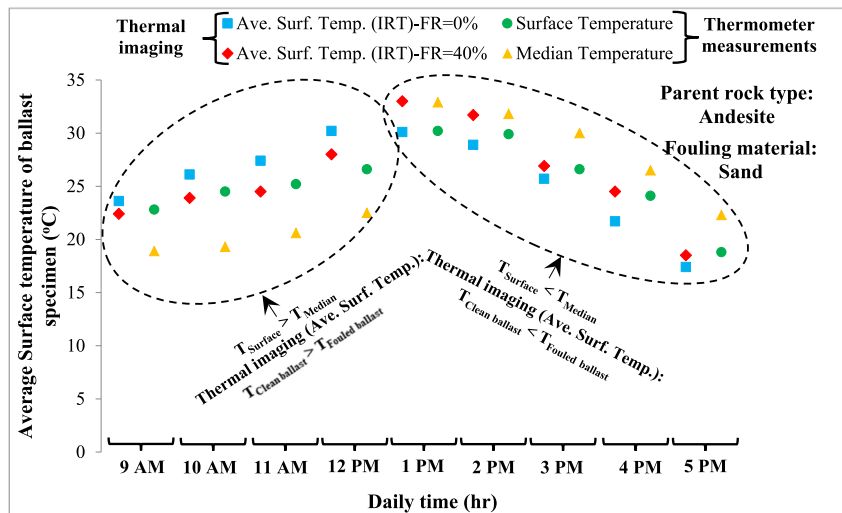
c Rock type: Andesite

Fig. 8. Surface temperature of ballast particles based on the thermal imaging and thermometer measurements considering clean and sand-fouled samples.
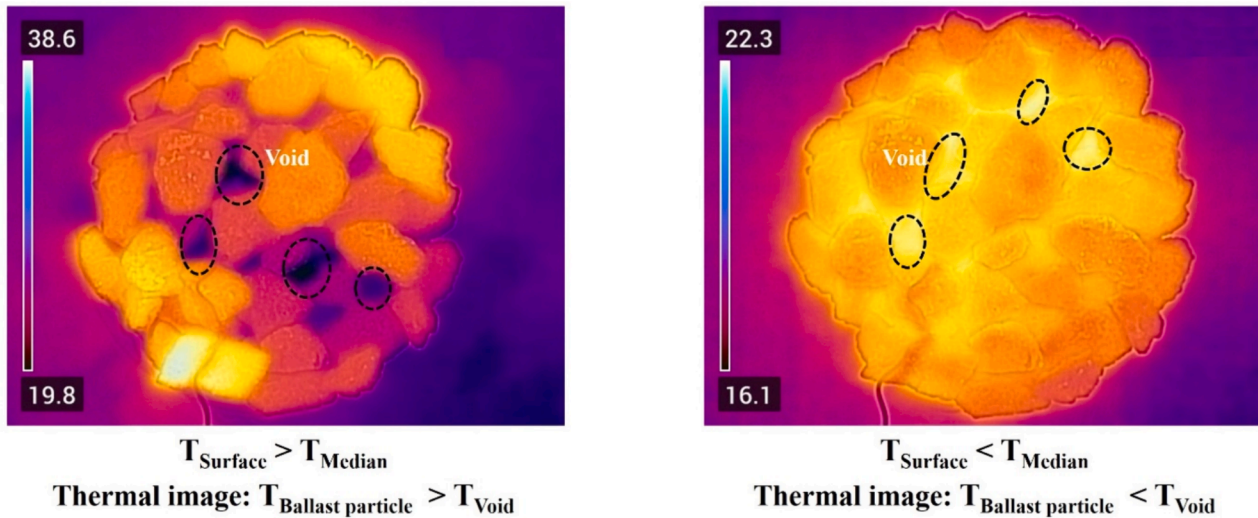
Fig. 9. Distinct temperature difference between ballast particles and voids considering temperature variation from upper surface towards lower layer.
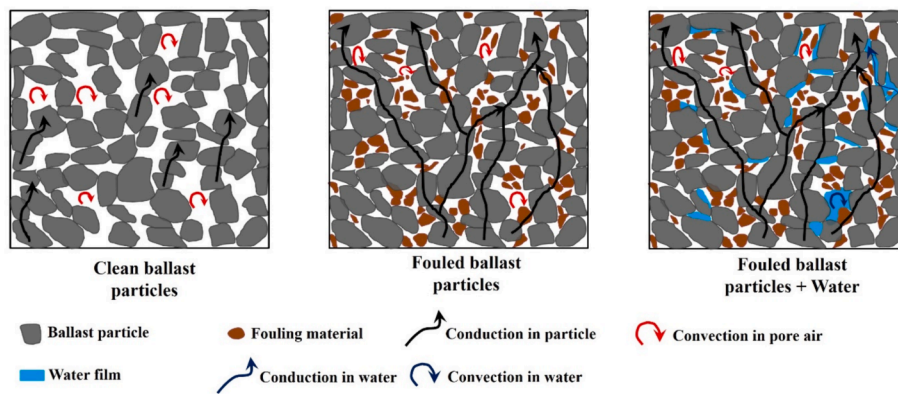
Fig. 10. Schematic layout representing thermal conductivity among ballast particles considering effect of fouling and moisture.

thermal dynamics within the sample.

Results and discussions

Effect of parent rock on thermal properties of clean ballast

The variety of rock types, especially those with distinct surface colors and water absorption capacities, offers valuable insights into how the physical characteristics of crushed particles affect the use of thermal imaging for measuring the temperature of ballast surfaces. This understanding is crucial for optimizing the use of IRT in railway maintenance and monitoring.

- The temperature readings captured by the IRT passive camera are consistent with those obtained from thermometers placed at both the mid-depth and the surface of the sample. This consistency supports the reliability of thermal imaging as a method for assessing ballast condition.
- As shown in Fig. 7, ballast from dark-colored rocks generally exhibits higher surface temperatures due to increased emissivity. Conversely, limestone, which is lighter in color, tends to have a lower surface temperature. This contrast is particularly pronounced during midday when solar radiation is strongest, enhancing the emissivity differences between different rock types.
- Further analysis of thermal images from individual ballast particles confirms the observed trends across the full samples. Generally,

darker rocks reflect less light and emit more thermal energy, while lighter rocks show opposite traits. For instance, andesite, with its rougher surface, has higher emissivity compared to the smoother surface of limestone, which reflects more light and emits less heat, as described by Vollmer and Möllmann [64].

Thermal properties of fouled ballast based on IRT

Effect of fouling

In this study, an initial investigation focuses on aligning the surface temperature readings from the IRT passive camera with those measured by thermometers installed at the surface and median depths. This comparison is crucial for verifying the accuracy of thermal imaging in real-world conditions.

As depicted in Fig. 8, during the morning hours (10 AM to 1 PM), fouled ballast generally shows a lower surface temperature compared to clean ballast when the surface temperature exceeds the median temperature. This finding suggests that fouling might insulate the surface somewhat from solar heating. Conversely, from 1 PM to 5 PM, as the temperature gradient reverses (surface temperature less than median temperature), fouled ballast tends to exhibit higher surface temperatures. This pattern indicates enhanced heat retention in the fouled layers, highlighting the optimal time frame for conducting thermal imaging to detect fouling effectively.

While some studies like those by Clark et al. [14] and Hosseini et al. [29] have found that fouled ballast can exhibit higher temperatures than

a Daily time: 10 AM

b Daily time: 12 PM

c Daily time: 1 PM

d Daily time: 4 PM
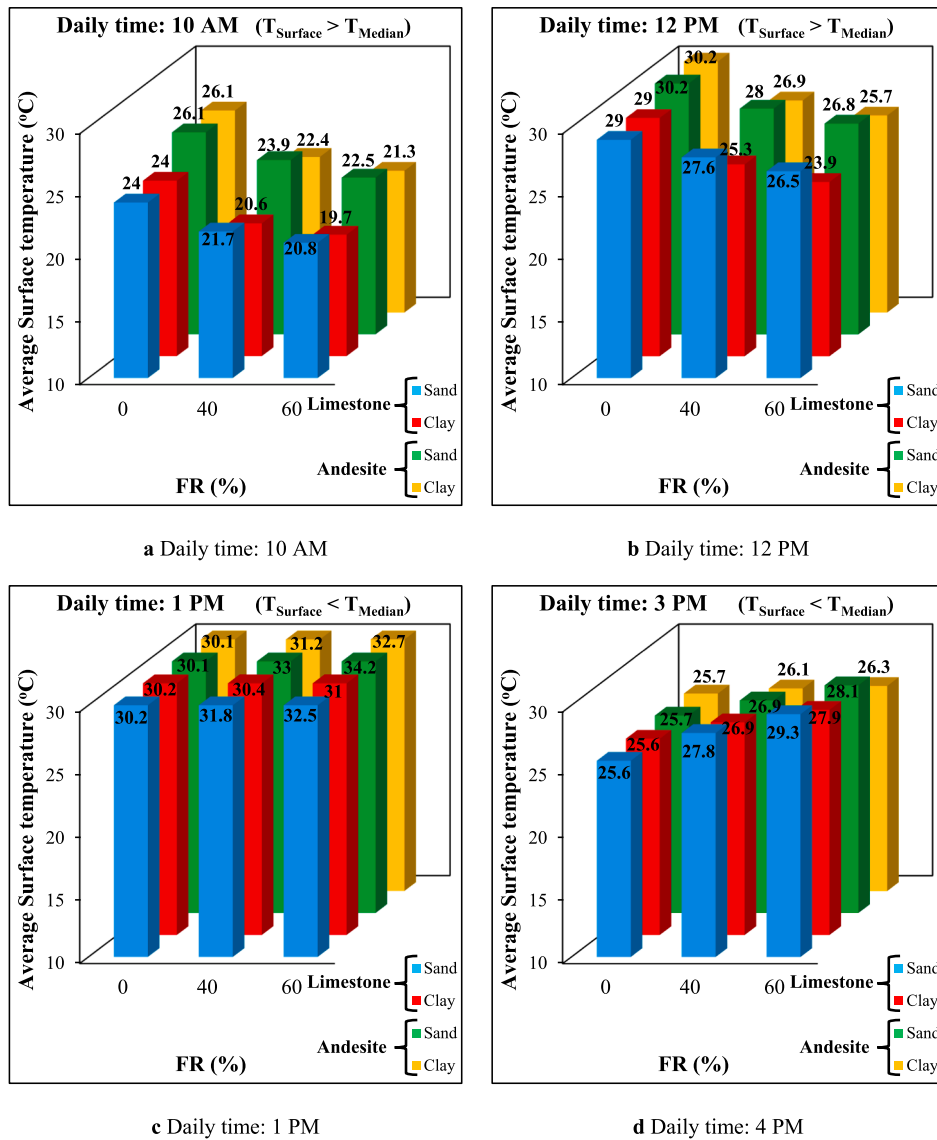
Fig. 11. Effects of fouling materials and fouling ratios on surface temperature of ballast samples contaminated with sand/clay.

Clean ballast

Partially fouled ballast: half thickness (FR=40%)

Fully fouled ballast: whole thickness (FR=40%) [Upper surface is clean]
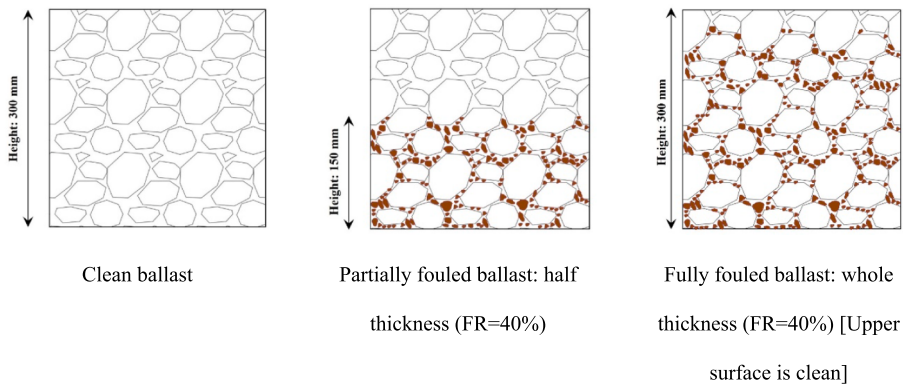
Fig. 12. Schematic illustration of fully fouled and partially fouled conditions compared to clean ballast.

clean ballast, others such as Liang et al.[39] and Tan et al. [59] report lower temperatures associated with higher levels of fouling. Advanced imaging techniques such as hyperspectral imaging have further elucidated these dynamics, revealing that fouling increases the reflectance but reduces the emissivity of the ballast-fouling mix, as per findings from Ichi and Dorafshan [31]. This alteration in physical properties due to fouling could explain the observed discrepancies in temperature readings.

As depicted in Fig. 9, the thermal imaging reveals a gradient in temperature between the voids and the granular particles (comprising
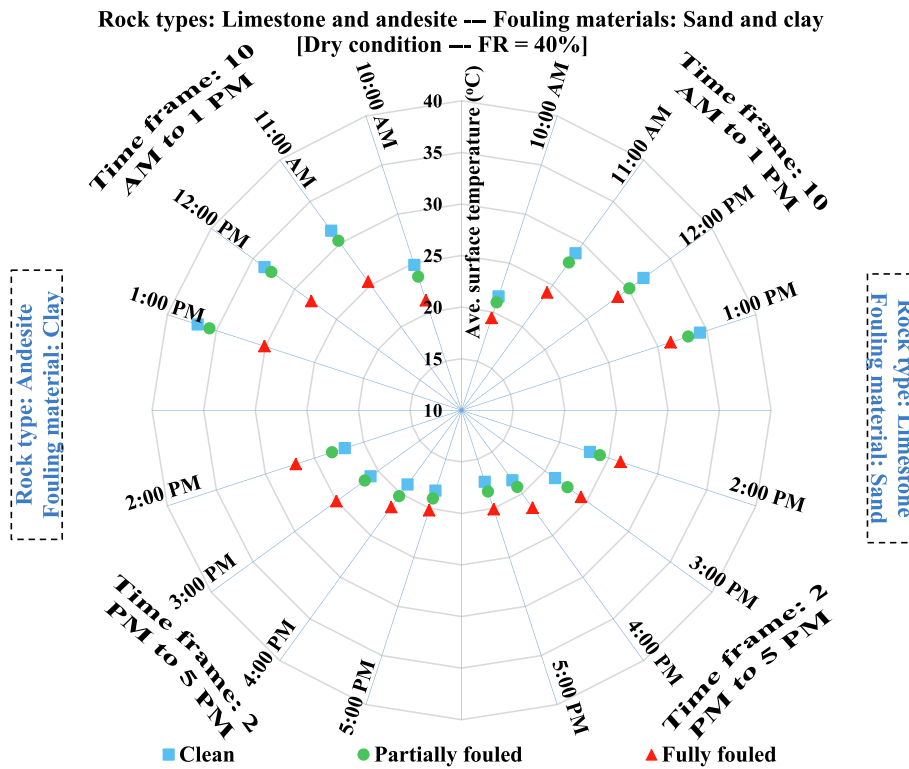
Fig. 13. Effects of fully fouled condition compared to partially fouled condition on surface temperature of fouled ballast.

ballast and fine fouling materials). This gradient is primarily due to variations in thermal conductivity, which significantly influence how heat is absorbed and dissipated within the structure.

During the initial period, as the air temperature rises and the materials are heated by the sun, the ballast particles absorb heat. This results in a higher recorded temperature in areas with fewer voids where heat is retained more effectively. Conversely, in the latter part of the day, these particles begin to release the absorbed heat. This phenomenon leads to a quicker decrease in temperature within areas that have a higher concentration of voids, as these regions have less capacity to retain heat.

This observation aligns with findings by Sabato et al. [55], who noted similar trends in thermal imaging studies for detecting subsurface voids in road infrastructures. On the other hand, Vazquez and Thomachot-Schneider [63] documented a slower cooling rate in fractured rock environments where the ambient temperature is lower than that of the rock itself. This slower rate is attributed to the reduced diffusivity of air in the cracks, which impedes heat flow and alters the thermal dynamics observed.

Density and particle size distribution (PSD) of granular media significantly influence their thermal conductivity, as these factors dictate the medium's ability to transfer heat [49]. Understanding these relationships is crucial for optimizing material properties in various engineering applications.

The primary mechanism for heat transfer in granular media is conduction through the granular skeleton. This pathway is heavily influenced by the density and arrangement of the particles within the medium.

According to Lyu et al. [44] and Zhang et al. [68], a mix of densely-packed fine and coarse particles tends to decrease the number of air pores. This reduction in porosity not only extends the paths for heat transfer but also increases the overall thermal conductivity by creating more contact points between particles. Additionally, as noted by Nguyen et al.[50], Haigh [28], and Alrtimi et al. [5], higher densities in granular mixtures reduce the amount of entrapped air, which is a natural insulator and thus a barrier to heat flow. This configuration enhances the

material's thermal efficiency.

Fig. 10 provides a schematic representation of these dynamics in granular materials such as ballast, illustrating how particle density and distribution affect thermal properties. Furthermore, the recent model by Zeng et al. [67] has quantitatively demonstrated how the presence of fine particles can alter the thermal conductivity of dry soils, providing valuable predictive capabilities for material design and assessment.

Effect of fouling materials and percentage

To evaluate the impact of different fouling materials and their concentrations on the thermal properties of ballast, Fig. 11 provides crucial visual data. It clearly shows that an increase in fouling content typically results in a more pronounced difference in surface temperature between clean and fouled ballast as captured by IRT. The nature of this temperature discrepancy—whether it increases or decreases—depends significantly on the specific time period during which imaging is conducted.

Research has indicated that higher fouling ratios enhance the thermal distinction between clean and fouled ballast across various depths, creating a more complex thermal profile that can be critically analyzed [60]. Additionally, differences in emissivity between particles and pores have been observed to affect surface temperatures, with areas of higher pore concentration showing warmer temperatures [51,47].

This analysis reveals that ballast fouled with clay generally exhibits lower surface temperatures than sand-fouled ballast. This observation aligns with the known thermal properties of these materials: sand has higher thermal conductivity but lower specific heat than clay, assuming equal moisture content and density [1,70]. Furthermore, Zhang et al. [69] have documented that larger particle sizes typically result in lower heat resistivity compared to finer grains, underscoring the role of particle size in thermal dynamics.

The thermal resistivity and capacity of the ballast are also influenced by the type of fouling material. For instance, rock minerals generally exhibit lower thermal resistivity than clay minerals due to different particle interactions. Over time, particularly when environmental temperatures and solar radiation decrease, fouled ballast—whether with
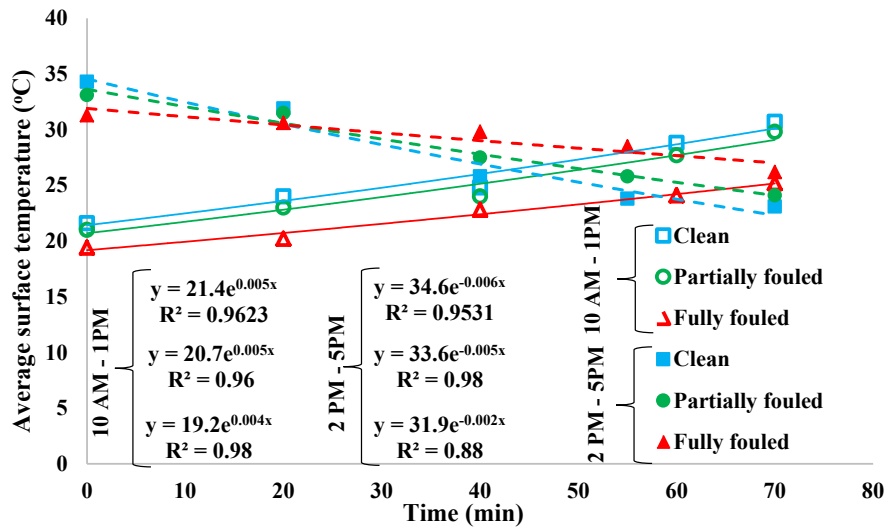
a Rock type: Limestone --- Fouling material: Sand
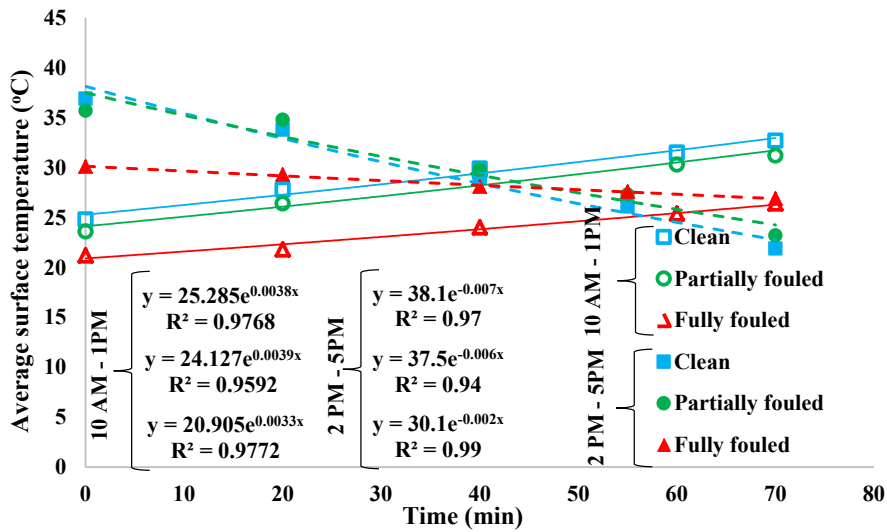
b Rock type: Andesite --- Fouling material: Clay

Fig. 14. Regression analysis on sequential thermal images considering clean as well as partially/fully fouled ballast.
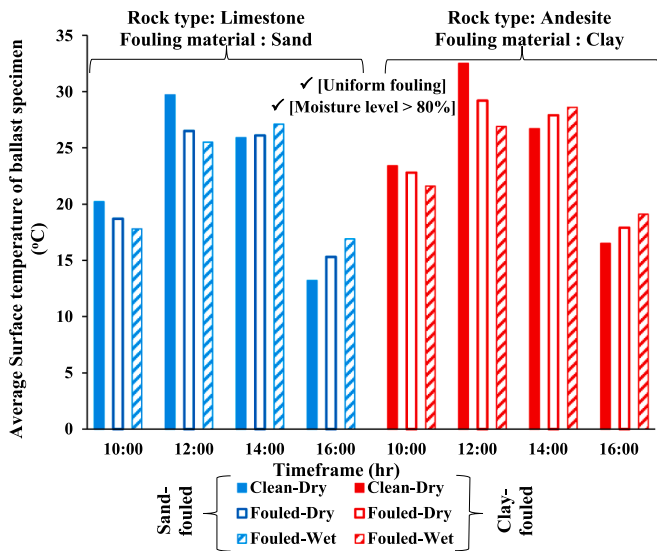
Fig. 15. Comparing IRT results for dry and wet samples of clean/fouled ballast.

sand or clay—tends to maintain higher temperatures than clean ballast.

Effect of partially/fully fouling intrusion in the ballast

IRT is used to detect variations in surface temperature of ballast, which are influenced by changes in density, porosity, specific heat capacity, and thermal conductivity of the subsurface. These factors collectively affect heat transport within the ballast layer [33]. Notably, if the fouling material is deeply embedded within the granular layer, far from the surface, the temperature contrast between clean and fouled samples becomes less discernible.

As illustrated in Fig. 12, experiments were conducted with samples of clean, partially fouled, and fully fouled ballast, each representing an equivalent fouling ratio but varying in the depth of fouling intrusion. The results, shown in Fig. 13, reveal that the temperature difference between partially fouled and clean ballast is not as pronounced as that between fully fouled and clean ballast. This suggests that shallow fouling does not significantly affect surface temperature, a finding supported by negligible temperature changes observed in the lower third of the granular layer.

Temperature comparisons further indicate that fouled ballast generally shows lower surface temperatures than clean ballast when the external temperature is high, and higher temperatures when external temperatures are low.

To elaborate on these temperature dynamics, thermal images were captured at different times (from 10 AM to 1 PM and from 1 PM to 5 PM), and regression analysis was applied to model the data (Fig. 14). This analysis confirmed that fouled ballast, particularly when the fouling reaches the upper layers, shows a moderated rate of temperature change due to its higher thermal mass. These observations are consistent with broader trends noted in previous studies (Fig. 8) and are aligned with Janků et al.'s [33] findings on thermal contrasts in concrete delamination, where visible temperature differences were linked to the physical properties of the materials involved.

Additionally, research by Mineo and Pappalardo [46] on the thermal properties of porous versus dense rock types has shown that porous materials tend to cool faster due to their greater surface area exposure and the presence of interconnected voids. These voids act as channels that facilitate heat flow from the warmer interior to the cooler exterior, further illustrating the complex thermal dynamics within different substrates.

Effect of moisture on thermal properties of fouled ballast based on IRT

Figs. 15 and 16 provide a comparative analysis of the average surface temperatures of clean and fouled ballast samples under both dry and moisturized conditions, across different rock types and fouling materials.

In general, moisturized fouled samples typically register lower temperatures when their surface temperature surpasses that of the surrounding ground. This trend reverses when the temperature gradient is inverted, i.e., when the temperature increases from the surface downwards. This differential behavior highlights the complex thermal dynamics influenced by moisture in the ballast. For clean ballast samples, both dry and wet conditions tend to produce similar IRT results. This consistency is attributed to the effective drainage capacity of clean ballast, which prevents water retention that could otherwise alter thermal readings.

The presence of moisture in soil particles within the ballast increases the overall thermal capacity, necessitating greater energy for heating or cooling to be detectable by surface thermal imaging. This effect is intensified by the increased volumetric heat capacity associated with higher bulk density and moisture content, as identified by Abu-Hamdeh [2]. Such conditions enhance the particle contact points, effectively creating thermal bridges that facilitate heat transfer.

According to Zhang et al.[69], soil samples with higher water content exhibit enhanced heat transfer capabilities due to the reduced thermal resistivity of water compared to air. This observation is consistent with findings by Persson [52] on heat transfer in granular media. The interaction between moisture and fouling materials (such as sand or clay) can improve thermal conductivity. This improvement occurs as moisture creates a conductive bridge across air gaps within the soil matrix, as shown schematically in Fig. 11. Conversely, Zhu et al.[70] reported that while thermal conductivity increases with density, it decreases as water content rises, suggesting an inverse relationship in less dense, water-rich environments. Similarly, Sass et al.[57] found that wet conditions generally lead to cooler surface temperatures.

Despite these general trends, the actual temperature readings of moisture-fouled ballast can vary depending on the specific environmental and air temperature conditions at the time of measurement.

Conclusions and perspectives

Conclusions

This study explored the efficacy of Infrared Thermography (IRT) for identifying ballast fouling, considering variables like parent rock type, fouling material, moisture levels, and fouling percentage. The key conclusions derived are as follows:

- Darker rocks such as andesite and basalt typically show higher surface temperatures compared to lighter rocks like limestone. This difference in temperature can be crucial for detecting changes in composition and potential fouling issues using IRT, making it a valuable tool for inspecting various types of ballast.
- IRT technology has demonstrated that fouled ballast often has a lower surface temperature than clean ballast when there is a decrease in temperature with depth. Conversely, when there is a temperature increase with depth, fouled ballast tends to exhibit higher temperatures. Additionally, a greater fouling ratio intensifies these temperature discrepancies, aiding in the detection of fouled conditions.
- Significant differences in surface temperature between dry and wet ballast samples, particularly with moisturized fouled ballast, highlight the effect of thermal capacity of water. This phenomenon indicates that moisture content is a critical factor in thermal imaging and can significantly influence IRT results.
- The research also underscores some limitations of IRT; specifically, it struggles to distinguish between clean and fouled ballast when the
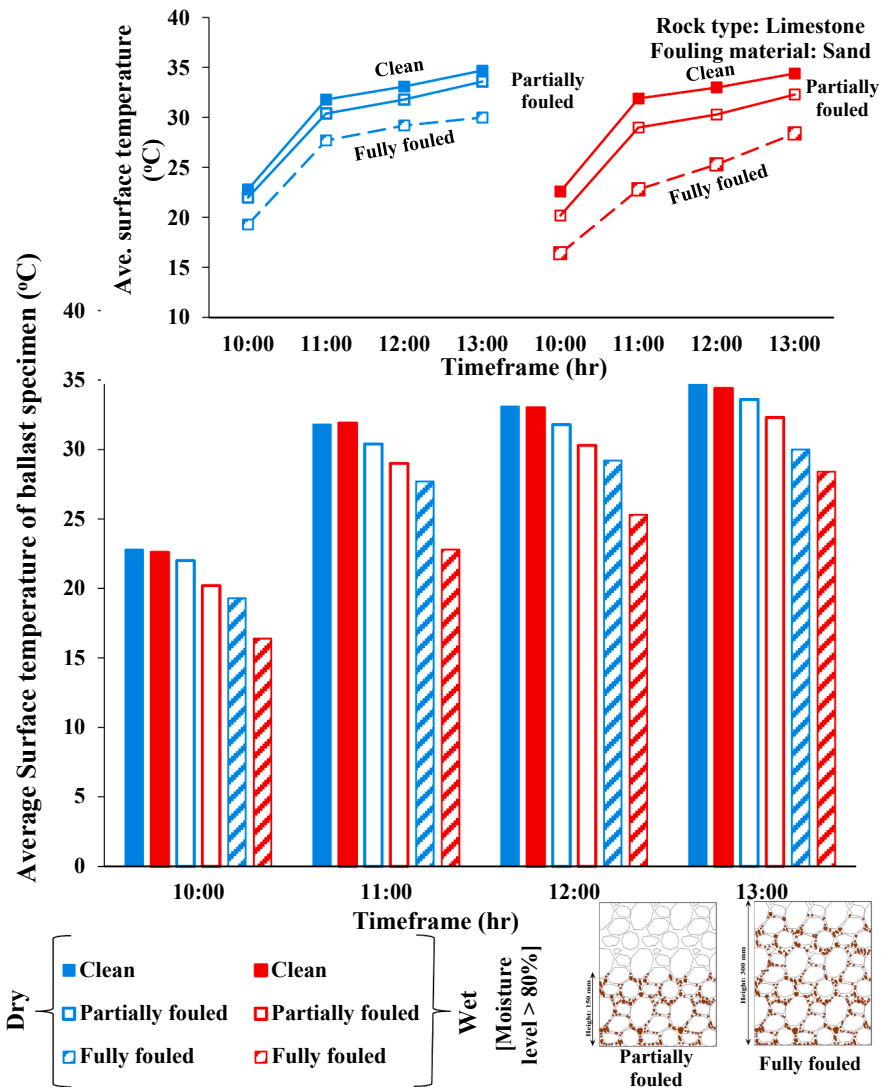
a Timeframe: Increment in air temperature [10 AM – 1 PM]

Fig. 16. Effect of moisture on IRT results considering clean ballast as well as partially/fully fouled ballast.
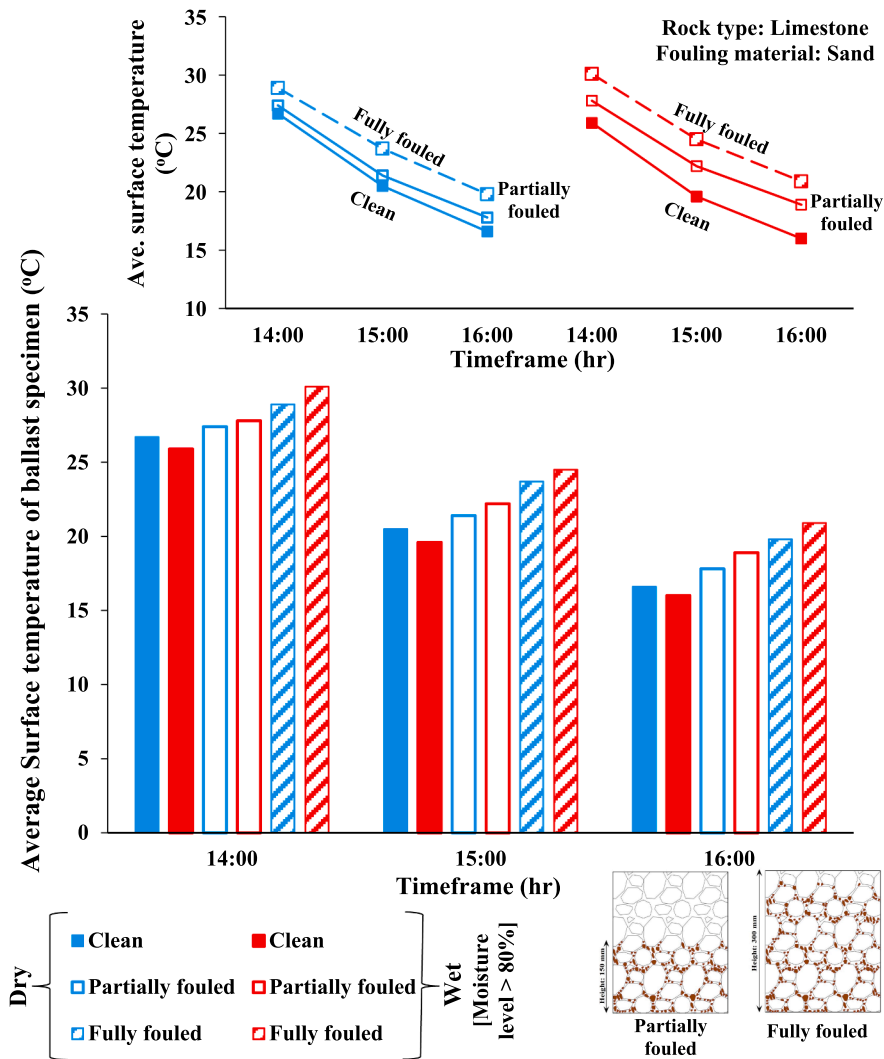
b Timeframe: Decrement in air temperature [2 PM – 5 PM]

Fig. 16. (*continued*).

fouling ratio is minimal (e.g., 20 % fouling ratio) or the fouling material is not deeply embedded (e.g., only reaching up to one-third of the ballast layer's lower thickness). This suggests that IRT's effectiveness may vary based on the extent and depth of fouling.

Future perspectives

This research has identified several challenges that need to be addressed to enhance the application of IRT in real-world scenarios.

- The variability in field conditions such as temperature fluctuations, the presence of water vapor, changes in solar radiation, variations in orientation of ballast layer towards sunlight direction, and the effectiveness of IRT in low-temperature environments must be further studied to improve the reliability of thermal imaging.
- Integrating machine learning algorithms, particularly convolutional neural networks (CNNs), could revolutionize the way images are processed. These technologies are capable of performing complex pattern recognition and classification tasks, including identifying different fouling ratios and distinguishing between various parent rock types. This approach would enhance the precision and efficiency of IRT analyses.

- Utilizing IRT passive cameras mounted on coaches or drones presents a promising method for conducting extensive field investigations. This setup allows for continuous monitoring of the railway infrastructure, potentially speeding up the detection and assessment of ballast fouling.
- Since IRT primarily provides surface-level data and does not give insights into the depth of structural defects, combining it with ground penetrating radar could offer a more comprehensive evaluation. This hybrid method would enable the detection of both surface and subsurface anomalies, thereby facilitating a more thorough assessment of track bed conditions. The integration of these technologies is especially pertinent in scenarios where the ballast surface is obscured, such as after rainfall, making it difficult to assess fouling directly from the surface.

CRediT authorship contribution statement

Mehdi Koohmishi: Writing – original draft, Software, Investigation, Data curation. **Sakdirat Kaewunruen:** Writing – original draft, Supervision, Methodology, Funding acquisition, Conceptualization. **Guoqing Jing:** Writing – original draft, Validation, Supervision, Investigation, Conceptualization. **Yunlong Guo:** Writing – original draft,

Visualization, Validation, Software, Resources, Methodology, Investigation, Funding acquisition, Conceptualization.

Declaration of competing interest

The authors declare that they have no known competing financial interests or personal relationships that could have appeared to influence the work reported in this paper.

Data availability

Data will be made available on request.

Acknowledgements

References

[1] Abu-Hamdeh NH. Thermal properties of soils as affected by density and water content. Biosyst Eng 2003;86(1):97–102.
[2] Abu-Hamdeh NH. Specific heat and volumetric heat capacity of granular materials as affected by moisture and density. Appl Mech Mater 2014;575:103–7.
[3] Akhloufi MA, Bendada A. May). Fusion of active and passive infrared images for face recognition. In: Thermosense: Thermal Infrared Applications XXXV, Vol. 8705. SPIE; 2013. p. 84–93.
[4] Almutawa N, Eid W. Soil moisture content estimation using active infrared thermography technique: An exploratory laboratory study. Kuwait Journal of. Science 2023.
[5] Alrtimi A, Rouainia M, Haigh S. Thermal conductivity of a sandy soil. Appl Therm Eng 2016;106:551–60.
[6] Astm c,. Standard test method for resistance to degradation of large-size coarse aggregate by abrasion and impact in the Los Angeles machine. West Conshohocken, PA: American Society for Testing and Materials; 2003. p. 535–1503.
[7] Astm c,. Standard test method for density, relative density (specific gravity), and absorption of coarse aggregate. West Conshohocken, PA: American Society for Testing and Materials; 2012. p. 127–1112.
[8] Barrett BE, Day H, Gascoyne J, Eriksen A. Understanding the capabilities of GPR for the measurement of ballast fouling conditions. J Appl Geophys 2019;169:183–98.
[9] Chang PC, Liu SC. Recent research in nondestructive evaluation of civil infrastructures. J Mater Civ Eng 2003;15(3):298–304.
[10] Chen L, Wang Y, Jia S, Siu MFF. Development of panoramic infrared images for surface temperature analysis of buildings and infrastructures. Energ Buildings 2021;232:110660.
[11] Ciampoli LB, Calvi A, D'Amico F. Railway ballast monitoring by GPR: A test-site investigation. Remote Sens (Basel) 2019;11(20):2381.
[12] Ciampoli LB, Calvi A, D'Amico F, Tostif F. In: GPR Data Collection and Processing Strategies for Railway Ballast Evaluation. IEEE; 2020. p. 426–9.
[13] Clark M, McCann DM, Forde MC. Infrared thermographic investigation of railway track ballast. NDT and E Int 2002;35(2):83–94.
[14] Clark M, Gordon M, Forde MC. Issues over high-speed non-invasive monitoring of railway trackbed. NDT and E Int 2004;37(2):131–9.
[15] Couchman MJ, Barrett B, Eriksen A. Synthetic modelling of railway trackbed for improved understanding of ground penetrating radar responses due to varying conditions. In: Near Surface Geophysics, 22(Special Issue: Ground Penetrating Radar (GPR) Numerical Modelling Research and Practice); 2024. p. 206–19.
[16] Dhakal N, Elseifi MA. Use of infrared thermography to detect thermal segregation in asphalt overlay and reflective cracking potential. J Mater Civ Eng 2016;28(2): 04015118.
[17] Elseicy A, Alonso-Díaz A, Solla M, Rasol M, Santos-Assunçao S. Combined use of GPR and other NDTs for road pavement assessment: An overview. Remote Sens (Basel) 2022;14(17):4336.
[18] Ferrante C, Bianchini Ciampoli L, Benedetto A, Alani AM, Tosti F. Non-destructive technologies for sustainable assessment and monitoring of railway infrastructure: a focus on GPR and InSAR methods. Environ Earth Sci 2021;80(24):806.
[19] FLIR (2014). User's manual, Publ. No.: T559795 in English.
[20] FLIR Thermal Studio (2023). User's manual FLIR thermal studio, https://www.flir.com/products/flir-thermal-studio-suite/.
[21] Fuentes S, Tongson E, Gonzalez Viejo C. Urban green infrastructure monitoring using remote sensing from integrated visible and thermal infrared cameras mounted on a moving vehicle. Sensors 2021;21(1):295.
[22] Garrido I, Lagüela S, Otero R, Arias P. Thermographic methodologies used in infrastructure inspection: A review—data acquisition procedures. Infrared Phys Technol 2020;111:103481.
[23] Germoglio Barbosa, I., Lima, A. D. O., Edwards, J. R., & Dersch, M. S. (2024). Development of track component health indices using image-based railway track inspection data. Proceedings of the Institution of Mechanical Engineers, Part F: Journal of Rail and Rapid Transit, 09544097231224825.
[24] Gong Y, Qian Y. Predicting Ballast Fouling Conditions Through RGB-Based Statistical Quantity Analysis. Transp Res Rec 2023;03611981231172938.
[25] Guo Y, Xie J, Fan Z, Markine V, Connolly DP, Jing G. Railway ballast material selection and evaluation: A review. Constr Build Mater 2022;344:128218.
[26] Guo Y, Wang S, Jing G, Yang F, Liu G, Qiang W, et al. Assessment of ballast layer under multiple field conditions in China. Constr Build Mater 2022;340:127740.
[27] Guo Y, Liu G, Jing G, Qu J, Wang S, Qiang W. Ballast fouling inspection and quantification with ground penetrating radar (GPR). International Journal of Rail Transportation 2023;11(2):151–68.
[28] Haigh SK. Thermal conductivity of sands. Geotechnique 2012;62(7):617–25.
[29] Hosseini, S., Tan, Y., & Ahmadian, M. (2020, April). Forward-looking infrared radiometry (FLIR) application for detecting ballast fouling. In ASME/IEEE Joint Rail Conference (Vol. 83587, p. V001T03A003). American Society of Mechanical Engineers.
[30] Huang H, Moaveni M, Schmidt S, Tutumluer E, Hart JM. Evaluation of Railway Ballast Permeability Using Machine Vision-Based Degradation Analysis. Transp Res Rec 2018;2672(10):62–73.
[31] Ichi E, Dorafshan S. Spectral characterization of fouled railroad ballast using hyperspectral imaging. Constr Build Mater 2023;394:132076.
[32] Indraratna B, Rujikiatkamjorn C, Salim W. Advanced rail geotechnology–ballasted track. CRC Press; 2023.
[33] Janků M, Cikrle P, Grošek J, Anton O, Stryk J. Comparison of infrared thermography, ground-penetrating radar and ultrasonic pulse echo for detecting delaminations in concrete bridges. Constr Build Mater 2019;225:1098–111.
[34] Koohmishi M, Kaewunruen S, Chang L, Guo Y. Advancing railway track health monitoring: Integrating GPR, InSAR and machine learning for enhanced asset management. Autom Constr 2024;162:105374.
[35] Kulkarni NN, Dabetwar S, Benoit J, Yu T, Sabato A. Comparative analysis of infrared thermography processing techniques for roadways' sub-pavement voids detection. NDT and E Int 2022;129:102652.
[36] Kulkarni NN, Raisi K, Valente NA, Benoit J, Yu T, Sabato A. Deep learning augmented infrared thermography for unmanned aerial vehicles structural health monitoring of roadways. Autom Constr 2023;148:104784.
[37] Kuo C, Shen T, Liu M, Yang S, Ji Z. Estimating the influence of saturation on investigating fouled railway ballasts using ground-penetrating-radar. In: IGARSS 2018–2018 IEEE International Geoscience and Remote Sensing Symposium. IEEE; 2018. p. 9359–62.
[38] Li D, Read D, Thompson H, Sussmann T, McDaniel R, Railway NS, et al. Annual Conference. FL: Orlando; 2010.
[39] Liang X, Niu X, Liu P, Lan C, Yang R, Zhou Z. Test on fouling detection of ballast based on infrared thermography. NDT and E Int 2023;140:102956.
[40] Liu G, Yang F, Wang S, Jing G, Nateghi Y. Railway ballast fouling, inspection, and solutions-A review. Proceedings of the Institution of Mechanical Engineers, Part F: Journal of Rail and Rapid Transit 2023;237(8):969–82.
[41] Loche M, Scaringi G, Blahůt J, Hartvich F. Investigating the Potential of Infrared Thermography to Inform on Physical and Mechanical Properties of Soils for Geotechnical Engineering. Remote Sens (Basel) 2022;14(16):4067.
[42] Loiotine L, Andriani GF, Derron MH, Parise M, Jaboyedoff M. Evaluation of infraRed thermography supported by UAV and field surveys for rock mass characterization in complex settings. Geosciences 2022;12(3):116.
[43] Luo J, Huang H, Ding K, Qamhia II, Tutumluer E, Hart JM, et al. Toward Automated Field Ballast Condition Evaluation: Algorithm Development Using a Vision Transformer Framework. Transp Res Rec 2023;03611981231161350.
[44] Lyu C, Sun Q, Zhang W, Geng J. A predictive model for the thermal conductivity of silty clay soil based on soil porosity and saturation. Arab J Geosci 2020;13:1–9.
[45] Milovanović B, Banjad Pečur I. Review of active IR thermography for detection and characterization of defects in reinforced concrete. Journal of Imaging 2016;2(2): 11.
[46] Mineo S, Pappalardo G. InfraRed Thermography presented as an innovative and non-destructive solution to quantify rock porosity in laboratory. Int J Rock Mech Min Sci 2019;115:99–110.
[47] Mineo S, Pappalardo G. Rock emissivity measurement for infrared thermography engineering geological applications. Appl Sci 2021;11(9):3773.
[48] Moaveni M, Wang S, Hart JM, Tutumluer E, Ahuja N. Evaluation of aggregate size and shape by means of segmentation techniques and aggregate image processing algorithms. Transp Res Rec 2013;2335(1):50–9.
[49] Mu J, Yu S, Hao S. Quantitative evaluation of thermal conductivity of earth materials with different particle size distributions. Renew Sustain Energy Rev 2023;184:113574.
[50] Nguyen TT, Picandet V, Carre P, Lecompte T, Amziane S, Baley C. Effect of compaction on mechanical and thermal properties of hemp concrete. Eur J Environ Civ Eng 2010;14(5):545–60.
[51] Pappalardo G, Mineo S. Investigation on the mechanical attitude of basaltic rocks from Mount Etna through InfraRed Thermography and laboratory tests. Constr Build Mater 2017;134:228–35.
[52] Persson BNJ. Heat transfer in granular media consisting of particles in humid air at low confining pressure. The European Physical Journal B 2023;96(2):14.
[53] Pozzer S, Pravia ZMC, Rezazadeh Azar E, Dalla Rosa F. Statistical analysis of favorable conditions for thermographic inspection of concrete slabs. J Civ Struct Heal Monit 2020;10(4):609–26.
[54] Pozzer S, Dalla Rosa F, Pravia ZMC, Rezazadeh Azar E, Maldague X. Long-term numerical analysis of subsurface delamination detection in concrete slabs via infrared thermography. Appl Sci 2021;11(10):4323.
[55] Sabato A, Yu T, Kulkarni NN, Dabetwar S. Detecting Subsurface Voids in Roadways Using UAS with Infrared Thermal Imaging, No. 22–025. Massachusetts: Dept. of Transportation. Office of Transportation Planning; 2022.

[56] Salvador P, Naranjo V, Insa R, Teixeira P. Axlebox accelerations: Their acquisition and time–frequency characterisation for railway track monitoring purposes. Measurement 2016;82:301–12.

[57] Sass O, Bauer C, Heil S, Schnepfleitner H, Kropf F, Gaisberger C. Infrared thermography monitoring of rock faces–Potential and pitfalls. Geomorphology 2023;439:108837.

[58] Schwarz K, Heitkötter J, Heil J, Marschner B, Stumpe B. The potential of active and passive infrared thermography for identifying dynamics of soil moisture and microbial activity at high spatial and temporal resolution. Geoderma 2018;327:119–29.

[59] Tan, Y., Chen, Y., Peterson, A. W., & Ahmadian, M. (2019, April). Monitoring and detecting fouled ballast using forward-looking infrared radiometer (FLIR) aerial technology: Possibilities and limitations. In *ASME/IEEE Joint Rail Conference* (Vol. 58523, p. V001T01A019). American Society of Mechanical Engineers.

[60] Tan, Y., Chen, Y., Hosseini, S. M., & Ahmadian, M. (2020, April). Simulation Evaluation of Fouled Ballast Thermal Characteristics. In *ASME/IEEE Joint Rail Conference* (Vol. 83587, p. V001T03A006). American Society of Mechanical Engineers.

[61] Tomita K, Chew MYL. A review of infrared thermography for delamination detection on infrastructures and buildings. Sensors 2022;22(2):423.

[62] Tran QH. Passive and active infrared thermography techniques in nondestructive evaluation for concrete bridge. AIP Conference Proceedings 2021;Vol. 2420, No. 1.

[63] Vazquez P, Thomachot-Schneider C. Infrared thermography as a tool to detect increasing cracking in granitic stones exposed to high temperatures. J Cult Herit 2023;59:163–70.

[64] Vollmer, M., Möllmann, K.P., (2017). Infrared Thermal Imaging. Fundamentals, Research and Applications. 2nd Edition, Wiley-VCH, 794 p.

[65] Wang Q, Xia R, Liu Q, Zhou H, Qiu J, Zhao B. Pixel-based thermal sequence processing algorithm based on R2 fractile threshold of non-linear fitting in active infrared thermography. Infrared Phys Technol 2020;109:103422.

[66] Ye XY, Luo YY, Li ZW, Liu XZ. A Quantitative Detection Method for Surface Cracks on Slab Track Based on Infrared Thermography. Appl Sci 2023;13(11):6681.

[67] Zeng S, Yan Z, Yang J. An improved model for predicting the thermal conductivity of sand based on a grain size distribution parameter. Int J Heat Mass Transf 2023;207:124021.

[68] Zhang N, Yu X, Pradhan A, Puppala AJ. Effects of particle size and fines content on thermal conductivity of quartz sands. Transp Res Rec 2015;2510(1):36–43.

[69] Zhang T, Cai G, Liu S, Puppala AJ. Investigation on thermal characteristics and prediction models of soils. Int J Heat Mass Transf 2017;106:1074–86.

[70] Zhu X, Gao Z, Chen T, Wang W, Lu C, Zhang Q. Study on the Thermophysical Properties and Influencing Factors of Regional Surface Shallow Rock and Soil in China. Front Earth Sci 2022;10:864548.